Electrical, Frequency and Thermal Measurement and Modelling of Supercapacitor Performance

Youssef Diab, Pascal Venet, Hamid Gualous, Gérard Rojat

Electrical, Frequency and Thermal Measurement and Modelling of Supercapacitor Performance

Yasser Diab*, Pascal Venet*, Hamid Gualous**, and Gerard Rojat*
* Université de Lyon, Lyon, F-69622, France ; université Lyon 1, Lyon, F-69622, France ; CNRS, UMR5005, CEGELY, Villeurbanne, F-69622, France.
** SET-FC-Lab UTBM-UFC, Bâtiment F, Rue Thierry Mieg, 90010 Belfort Cedex, France
yasser.diab@gmail.com

***Abstract*—This paper presents an evaluation of commercial supercapacitors performance (*ESR*, *C*, self-discharge, P_{max}, E_{max}, coulumbic efficiency, etc), under different conditions. Characterization of supercapacitor performances as a function of current, voltage, frequency and thermal constraints, is carried out by constant current test, electrochemical impedance spectroscopy, and voltamperometry. A comparative study of measurement techniques is conducted in detail in this work. The supercapacitor self-discharge amplitude is determined by measuring the decline of open-circuit voltage. The mechanisms of the self-discharge, leakage current and diffusion of ions at the electrode-electrolyte interfaces are modelled by a new electrical equivalent circuit. In addition, we model the electrochemical impedance of self-discharge with diffusion-controlled in frequency domain. Supercapacitor is represented by two complementary electrical equivalent circuits: two branches and non-homogeny pores. The first represents the supercapacitor time behaviour. The second represents supercapacitor dynamic behaviour. Finally, the origin and a new model of pseudo-inductance are described.**

***Keywords*: Characterisation techniques, supercapacitor characteristics, coulumbic efficiency, self-discharge modelling, pseudo-inductance modelling.**

1. INTRODUCTION

The determination of supercapacitors parameters under conditions recreated in laboratory can predict their behaviours in industrial applications. Supercapacitors generate variable and superimposed physical phenomena. Supercapacitors characterization methodologies are not standardized and it is difficult to compare the results obtained with those of manufacturers. At present time no international standards are existed. The results are depending on different parameters as ambient temperature, current intensity, frequency and voltage. Therefore, reliable and reproductive experimental results are required; we propose in this paper a comparative study on measurement methods applied on MAXWELL commercialized supercapacitors (see tab. 1).
In addition, we need a whole equivalent circuit model for representation supercapacitor phenomena in power electronics simulation. So, we use and compare two complementary models: two branches and non-homogeny pores, in frequency domain. We develop, in this paper, new equivalent circuits for pseudo-inductance and self-discharge phenomena.

Component	BCAP010	BCAP013	BCAP0350	MC2600
Rated Capacitance C_R (kF)	2.6	0.45	0.35	2.6
Rated voltage U_R (V)	2.5	2.5	2.5	2.7
Rated current I (A)	600	180	30	600
Leakage current I_{lem} (mA)	5 12h	3 72h	1 72h	5 72h

Tab. 1: Studied supercapacitors parameters as given in manufacturer's datasheet

2. DC CHARACTERISATION AND MODELLING

5.1. Classical equivalent RC circuit

Supercapacitor performance can be approximated by the first order response of RC circuit. This model includes an equivalent series resistance (*ESR*) and an ideal capacitance (*C*). There are several measurement methods able to determine the both parameters (*C* and *ESR*). One of which is the standard. The voltage across the supercapacitor is maintained at its rated value U_R during 1h then the supercapacitor is discharged with constant current *I*. The capacitance determination, *C*, was made during DC discharge between $0.8U_R$ and $0.4U_R$ according the linear relation $C=I.\Delta t_c/\Delta U_c$. The *ESR* can be determined at the start of discharge by $ESR=\Delta U_0/I$. The voltage drop ΔU_0 is calculated as the intersection of extrapolated curve of experimental voltage and the straight of instantaneous voltage drop, occurred when the supply current is switched on (see fig. 1) [1-3].

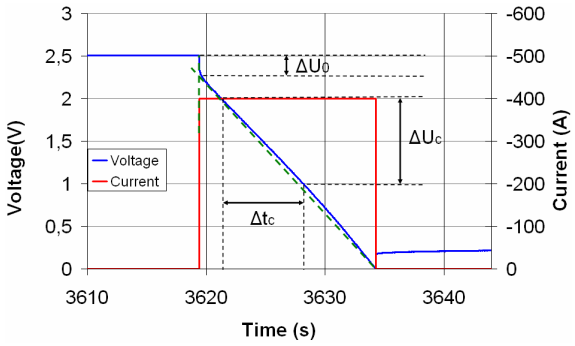

Fig. 1: Determination of supercapacitor parameters

Therefore, this method results depend on discharge current as shown in fig. 2: The capacitance, *C*, varies slightly but the *ESR* increases considerably with a reducing of current.

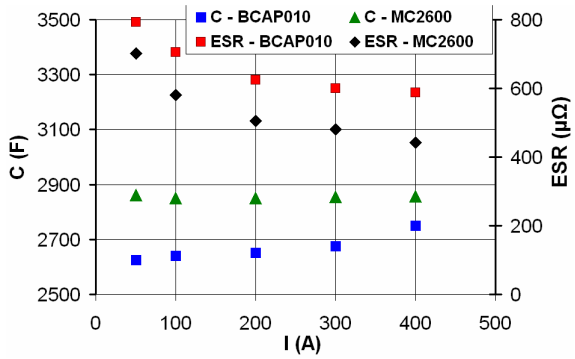

Fig. 2: Characterisation of supercapacitor parameters by standard technique

5.2. Two branches model

A method of determining supercapacitor parameters is to perform constant-current charging or discharging. This method consists in representing of a supercapacitor by two time constants immediate and delayed branches. The supercapacitor equivalent circuit can be represented by fig. 3. The immediate parameters can be identified carrying out a high charge/discharge current. .

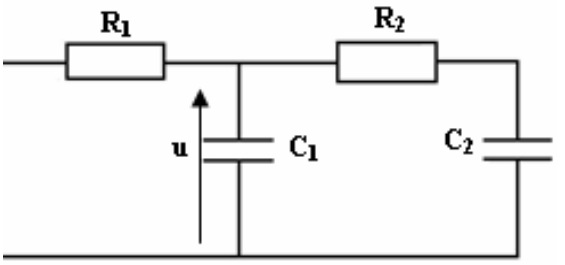

Fig. 3: Two branches model [4]

The differential capacitance $C_1(u)$ is presented by two capacitances: a constant capacitance C_0 and a linear voltage-dependent capacitance k as given in equation 1 [4]:

$$C_1(u) = C_0 + k.u \quad (1)$$

The resistance R_1 can be determined by the ratio of voltage drop at the beginning of charging to current. The constant C_0 in the equation 1 can be determined from the definition of differential capacity $I/du(0)/dt$ determined near to initial instant of charging. The slope k can be identified by the evolution of voltage ΔU_t and Q=I. Δt_t charge of supercapacitor stored during charging as follow [4]:

$$k = \frac{2\,(I.\Delta t_t - C_0 \cdot \Delta U_t)}{\Delta U_t^{\,2}} \quad (2)$$

We founded experimentally that the R_1 is practically constant but, the capacitance $C_1(u)$ elements depend on the rate of charge/discharge current (e.g. the component BCAP010 see fig. 4). This difference between the charge and discharge capacitance is probably due to Faradic current (redox) [5] and to charges trapped in pores with low accessibility.

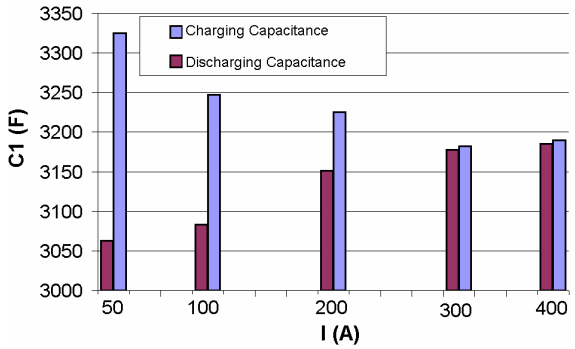

Fig. 4: Capacitance dependence on rate of charge/discharge current

5.3. Coulumbic (discharge/charge) efficiency

In order to quantify the difference between the discharge and charge capacitance, we define a factor called coulumbic efficiency. The last represents the discharge capacitance relative to that of charge for the rated voltage. Its variation with charge/discharge current is shown in fig. 5 for the component BCAP010.

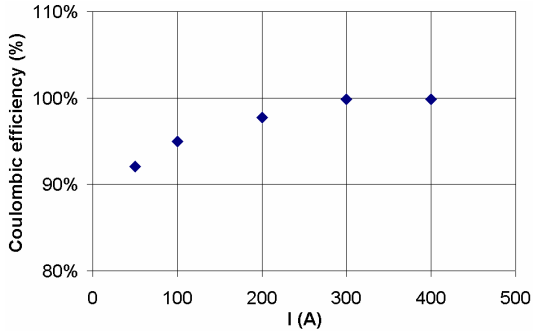

Fig. 5: Coulumbic efficiency vs. charge/discharge current

5.4. Voltamperometry measurement

This method is based on the current measurement resulting from a linear potential sweep dU/dt between two chosen limits U_1 and U_2. It allows directly determining the capacitance [6].

The variation of coulumbic efficiency with cycle number for Maxwell supercapacitors is shown in fig. 6. The capacitance determination for the studied supercapacitors was done with the same relationship capacitance-sweep. The increase of coulumbic efficiency during subsequent cycling is attributed to irreversible phenomena [7].

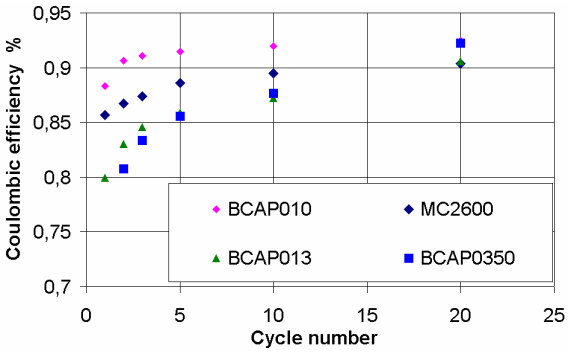

Fig. 6: Coulumbic efficiency vs. cycling number

5.5. Ragone plot

Ragone plots provide the available energy of a supercapacitor for constant power request [8,9]. Fig. 7 shows the Ragone plot for two Maxwell supercapacitors. The supercapacitors are charged as described above during 1h (see § 5.1) then they are discharged with constant power from U_R to $U_R/2$.

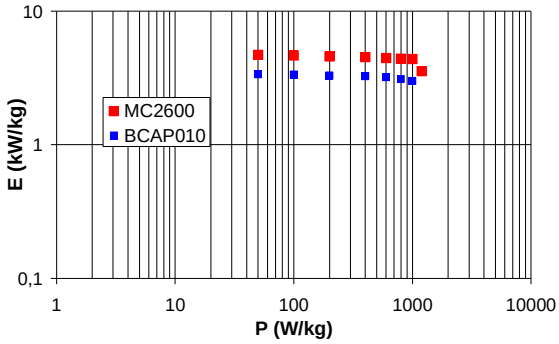

Fig. 7: Ragone plot of supercapacitors

3. FREQUENCY MEASUREMENT AND MODELLING

3.1. Frequency model

Electrochemical impedance spectroscopy (EIS) is used for the electrical/ electrochemical characterization of supercapacitors. Its different parameters R_s high frequency resistance, R_{el} electrolyte resistance, inductance L_s, low frequency capacitance C_{dl}, etc, can be determined independently in different frequency ranges [10]. An electrical equivalent model can be represented as shown in fig. 8 with a finite number n of RC cells. The resistance R_n and C_{dln} are calculated by eq. 3.

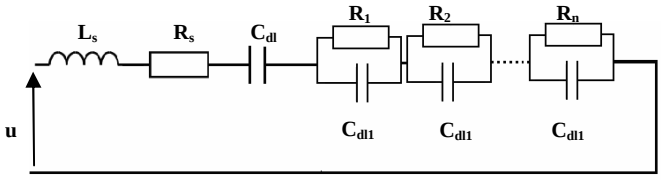

Fig. 8: Impedance pore model [10]

$$R_n = \frac{2\tau}{n^2\pi^2 C_{dl}} \; ; \; C_{dl\,n} = C_{dl}/2 \qquad (3)$$

Fig. 9 shows the impedance diagram in Nyquist plan for the different models. The finite number of cells and non-homogeny pores on the electrodes makes the model (impedance pore model) less accurate. The half-order model has been called to represent the non-homogeny pores at the electrodes phenomenon [11] (see fig. 9). This model allows developing the coth term of eq. 4 (left side) to secondary order as follows:

$$Z_p(\omega) = \frac{\tau.\coth(\sqrt{j\omega\tau})}{C_{dl}.\sqrt{j\omega\tau}} \Rightarrow Z_p(\omega) \cong \frac{\sqrt{1+j\tau.\omega}}{j\omega.C_{dl}} \qquad (4)$$

In order to take into account non-homogeny pores phenomenon in impedance pore model, we can use the fitting. The resulting model is called the non-homogeny pores model. This model represents a trade-off between precision and simplicity and can be used to model supercapacitors in power electronics simulation.

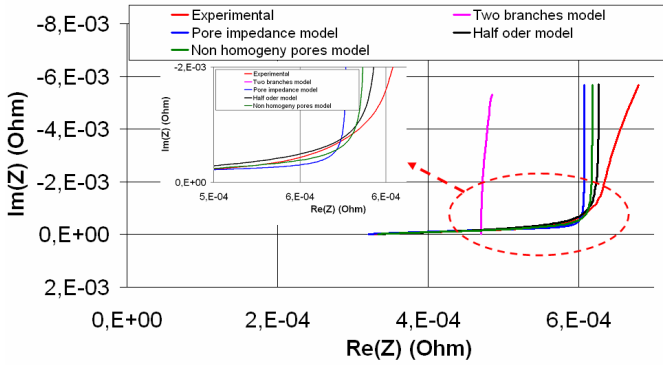

Fig. 9: Comparison between the different models in Nyquist diagram

It is essentially the self-inductance of the conductive loop formed by the terminals, connectors and electrodes of the cell inductive behaviour can also result from non-homogeneous current distribution [12] and electrochemical reactions at supercapacitor [13,14]. In these cases, it represents an error in the EIS measurement; this is why it should be represented in the equivalent circuit (see fig. 9).

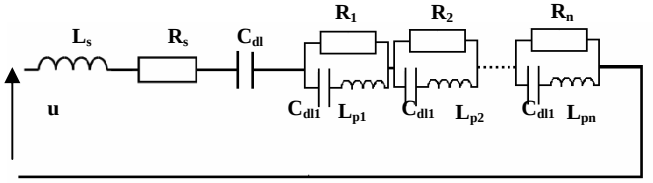

Fig. 10: Supercapacitor complex pore model tacking into account pseudo-inductance

In order to validate experimentally the established model, we carried out a high frequency test by EIS from 60 Hz to 10 kHz (for component BCAP010). We compare in Nyquist diagram (see fig. 11) the experimental result with the two models. The first is schematized on fig. 8 with a simple inductance and the second is schematized on fig. 10. We observe the proposed model improve very much the supercapacitor frequency response.

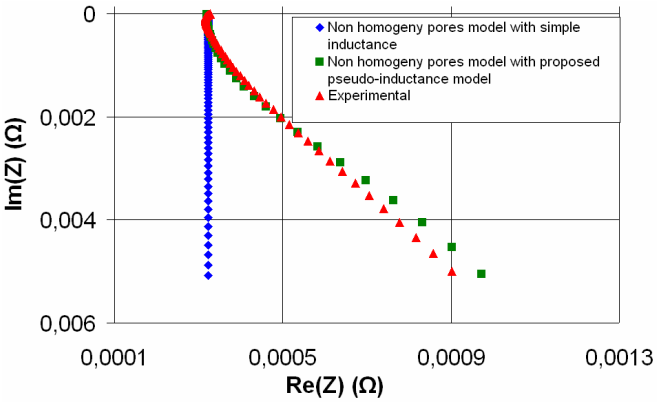

Fig. 11: Comparison of the proposed model of pseudo-inductance with experimental curve

4. COMPARISON OF MEASUREMENT TECHNIQUES

From fig. 12, we constant that, on the one hand, the capacitance measured by EIS is generally lower than that obtained by the two transit techniques: charge/discharge with constant current and voltamperometry. This is due to the Faradique charges generated by redox which can take place during the charge. During the discharge (Faradique effect is practically non present), the results obtained by voltamperometry approach to those obtained by EIS. One the other hand, for tensions higher than 0.5 V, we find a good agreement between the capacitance values obtained by the two last techniques (see fig. 12).

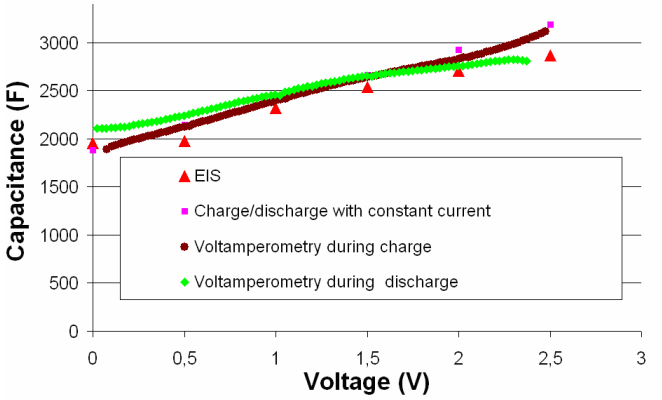

Fig. 12: Capacitance voltage dependence by different techniques

In order to compare the different techniques of measurement, the nominal capacitance is determined by the mean of the capacitance between U_R and $U_R/2$ [15]. The results of the aforementioned techniques are compared in tab. 2.
The capacitance values obtained both by impedance spectroscopy and by DC characteristics (discharge of voltamperometry and Norm) are in a good agreement, while the methods charge/discharge with constant current (C_1) and voltamperometry give higher values.

Capacitance (F)		Charge/discharge (400A)	EIS	Voltampero-metry (10 mV/s)		Standard	
				Charge	Discharge	400 A	50 A
	C_R	*2600*	*2600*	*2600*	*2600*	*2600*	*2600*
BCAP010	**C**	2863	2614	2792	2596	2750	2623
	C/C$_R$	110%	101%	107%	100%	106%	101%
MC2600	**C**	3130	2842	2956	2869	2857	2861
	C/C$_R$	120	109	114	110	110	110

Tab. 2: Comparing of nominal capacitance values

We can distinguish in manufacturer's documentation two resistances: DC resistance. (determined by discharge with high constant current) and AC resistance (determined for a given frequency). We present in the tab. 3 the different resistances of supercapacitor relative to that given by manufacturer. We can observe that the resistance values are dispersed; each method gives a value different from the others, but measurements by the methods standard and EIS (low frequency) give close values.

Resistance (µΩ)		EIS		Standard		Charge/discharg (400A)
		Rs (φ=0°)	ESR 55mHz	400 A	50 A	
BCAP010	**ESR**	*322*	*620*	*587*	*792*	*447*
	ESR$_R$ (DC)	*700*	*700*	*700*	*700*	*700*
	ESR/ESR$_R$ (DC)%	46	89	84	113	64
	ESR$_R$ (1kHz)	*300*	*300*	*300*	*300*	*300*
	ESR/ESR$_R$ (1kHz)%	*107*	*201*	*196*	*264*	*149*
MC2600	**ESR**	*272*	*439*	*422*	*701*	*360*
	ESR$_R$ (DC)	*400*	*400*	*400*	*400*	*400*
	ESR/ESR$_R$ (DC)%	69	110	106	175	90
	ESR$_R$ (100Hz)	*280*	*280*	*280*	*280*	*280*
	ESR/ESR$_R$ (100Hz)%	97	157	150	250	129

Tab. 3: Comparing of resistances values

5. SELF-DISCHRAGE CHARACTERISATION AND MODELING

5.1. Self-discharge measurements

It has been found that a gradual decrease in voltage across the charged supercapacitor occurs in long term open-circuit. This is due to self-discharge. In this case, the self-discharge has two mechanisms: leakage current and diffusion of ions at the electrode-electrolyte interfaces [16,17]. The second is called the self-discharge with diffusion-controlled. The self-discharge can be characterized by measuring the decline of open-circuit voltage of the supercapacitor.

In order to limit the relaxing phenomena effect on the self-discharge measurement, the supercapacitor is charged with a constant voltage supply for one hour. After one hour, all the components of the supercapacitor are approximately charged to the same voltage, assuming that the relaxing phenomena have time constants of less than one hour. Consequently, when the charging current is stopped, the decrease in voltage across the supercapacitor follows only the effect of self-discharge [16].

Fig. 13 shows the self-discharge of the aforementioned supercapacitors at an ambient temperature of 25 °C and for an initial voltage of 2.5 V. It illustrates that the self-discharge rates of components are different. It is noticed that the components MC260 has the highest self-discharge rates, whereas the components BCAP010 has the smallest rate.

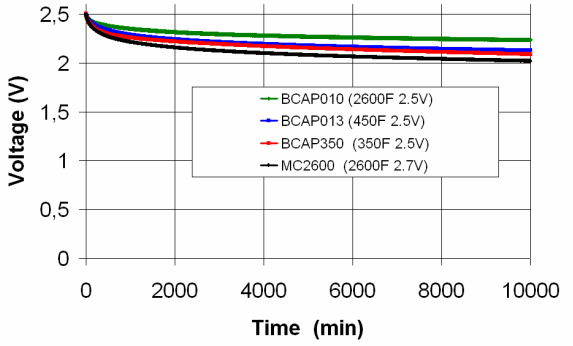

Fig. 13: Self-discharge rate of studied supercapacitors

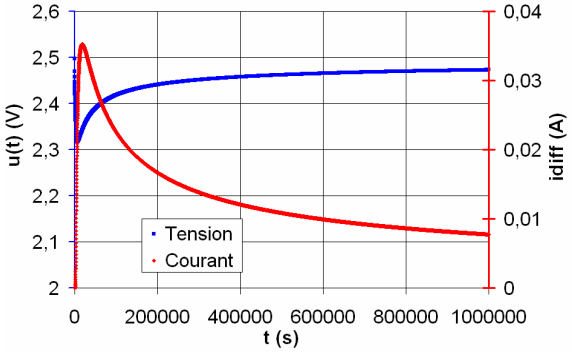

Fig. 14: Evolution of supercapacitor voltage and current during self-discharge

5.2. Self-discharge modelling

The self-discharge with diffusion-controlled is due to Faradic impurity reactions and it dominates the self-discharge during several hours (3h to 45h) [18]. From the diffusion equation of charges concentration at the interfaces carbon-electrolyte, we can deduce the supercapacitor current and voltage during the self-discharge [16] (for BCAP010 is less than 10 h) (see eq. 5 and 6).

$$i_{diff}(t) = m.C.\exp\left(\frac{-{h_0}^2}{Dt}\right) \quad (5)$$

$$u(t) = U_0 - m\left[\sqrt{t}\left(1-\exp\left(\frac{-{h_0}^2}{Dt}\right)\right) + h\sqrt{D}\,erfc\left(\frac{h_0}{\sqrt{Dt}}\right)\right] \quad (6)$$

Where, U_0 *is* the initial voltage across the supercapacitor. $2h_0$ is the thickness of a region of electrolyte immediately adjacent to each electrolyte-carbon interface of the supercapacitor. m is the diffusion parameter which can be calculated by equation 4 [16].

$$m = \frac{C_{R0}q\sqrt{D}}{C_{12}\sqrt{\pi}} \quad (7)$$

where D is the diffusion coefficient of the ions in the electrolyte. C_{12} is the series combination of the capacitances at the two interfaces of the capacitor, per unit area of one of the interfaces. C_{R0} is the initial ionic species concentration at the electrode-electrolyte interfaces. Also, q is the charge carried to the carbon surface by each ion [16]. These parameters can identified by a physico-chemical analysis of supercapacitor electrolyte.

Fig. 14 shows the evolution of current and voltage during the self-discharge with diffusion-controlled. We obverse the voltage across the supercapacitor firstly decreases during several hours, and then it comes back very slowly to its initial value U_0 during several days. The increase in a supercapacitor voltage is called recovery voltage phenomenon.

From the theory of self-discharge with diffusion-controlled and by using Laplace transform, we could deduce an electrochemical impedance model (see eq. 8).

$$Z(\omega) = -\frac{-\frac{h.BesselI\left(1,\frac{2h.\sqrt{j\omega}}{D}\right)}{j\omega.\sqrt{D}} - \frac{jh^2.BesselI\left(0,\frac{2h.\sqrt{j\omega}}{D}\right)}{D.\omega} + \frac{h^2.Dirac(j\omega)}{D}}{C} \quad (8)$$

Nevertheless, this model requires some physical parameters which are difficult to determine and to be established in time domain. We propose modelling the self-discharge with diffusion-controlled and leakage current by the equivalent circuit depicted in fig. 15. The equivalent circuit elements R_{le}, R_r and C_r can be determined by time behaviour of self-discharge.

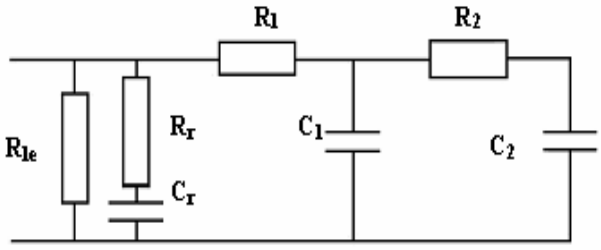

Fig. 15: Proposed equivalent circuit of self-discharge

5.3. Experimental approach

The circuit shown in fig. 15 demonstrates that part of the charge stored immediately in capacitance C_1 will be redistributed into capacitance C_2 and C_r. C_2 has a negligible effect. The phenomenon of the redistribution is relatively low because the capacitor is charged during an hour. When the supply current is stopped the charge Q_0 stored in C_1 will be diffused to C_r as the C_r has an almost zero voltage. At the end of the diffusion-controlled, both capacitances, C_1 and C_r, will have the same voltage, U_r, with total charge, Q_r. The capacitance C_r can be determined by using the charge balance:

$$Q_r = Q_0 \quad (9)$$

where,

$$Q_r = U_r.(C_1(U_0) + C_r)$$
$$Q_0 = U_0.C_1(U_r) \quad (10)$$

As a result, $C_r = \frac{C_1(U_0).U_0 - C_1(U_r).U_r}{U_r}$ **(11)**

The circuit schematised on the figure 15 can be reduced to that shown in the figure 16 during the self-discharge with diffusion-controlled

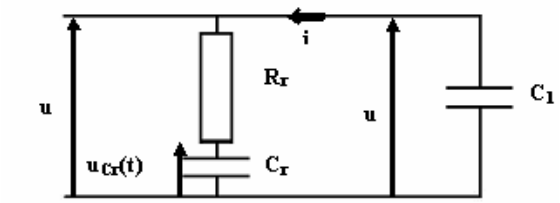

Fig. 16: Equivalent circuit of capacitor during self-discharge with diffusion-controlled

From this figure, we can write the following equations:

$$u(t) = i(t).R_r + u_{c_r}(t)$$
$$i(t) = C_r \frac{du_{Cr}(t)}{dt} = -C_1 \frac{du(t)}{dt} \quad \textbf{(12)}$$

Thus, we can deduce the time evolution of supercapacitor voltage during the self-discharge with diffusion-controlled:

$$C_1 R_r \frac{d^2u(t)}{dt^2} + \frac{C_1 + C_r}{C_r}\frac{du(t)}{dt} = 0 \quad \textbf{(13)}$$

The solution of the above equation with presented initial conditions can be estimated by the equation

$$u(t) = U_0 \exp\left(-\frac{t}{\tau_r}\right) \quad \textbf{(14)}$$

τ_r is the constant time of self-discharge due to diffusion-controlled, which can be calculated with the following equation :

$$\tau_r = \frac{C_1 C_r R_r}{C_1 + C_r} \quad \textbf{(15)}$$

Assuming that the capacitance $C_1 >> C_r$ the time constant can be reduced as follow:

$$\tau_r = C_r R_r \quad \textbf{(16)}$$

The time constant of the exponential described in equation 16 was determined experimentally by fitting (with software of non-linear least squares fit) of the experimental result for the first hours. The resistance R_r ascribed to the evolution of Faradic reactions at the electrode-electrolyte interfaces can be calculated by equation 17. Equivalent parallel resistance R_{le} will impact long term storage performance because it is basically a leakage effect. The last can be negligible compared with the self-discharge with diffusion-controlled within the first hours

$$R_r = \frac{\tau_r}{C_r} \quad \textbf{(17)}$$

Equivalent parallel resistance R_{le} will impact long term storage performance because it is basically a leakage effect. In this case, the voltage across the capacitor decreases as an exponential function of time as follows:

$$u(t) = U_r \exp\left(-\frac{t}{\tau_{le}}\right) \quad \textbf{(18)}$$

where τ_{le} is the time constant of leakage current. The time constant is determined experimentally; the decline of open-circuit voltage is approximated by an exponential function. The Faradic leakage resistance R_{le} is calculated as follows:

$$R_{le} = \frac{\tau_{le}}{C_1(u)} \quad \textbf{(19)}$$

There is a slight difference between the circuit simulation and the experimental results (1.2 % mean relative error) (see fig. 17). The experimental results demonstrate the self-discharge can be entirely represented by an equivalent circuit with low error. This circuit is more advantageous than the analytical model described in the previous section because it is easy to be established, and allow estimating the magnitude of the electrochemical storage of energy in electrical double layer capacitor.

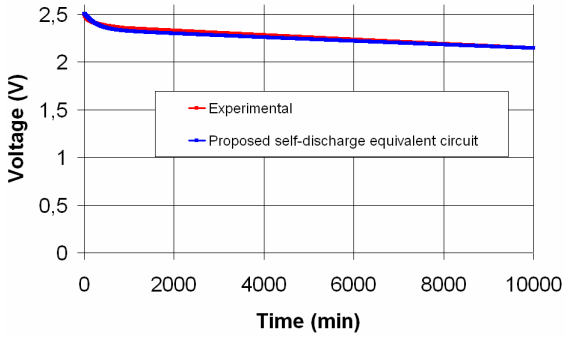

Fig. 17 : Comparison of the equivalent circuit of the self-discharge with experimental

Tab. 4 shows the self-discharge parameters normalized to those given in the manufacturer's datasheet. We remark: the capacitance C_r rises with an increase in capacitance of supercapacitor because the redox increases with an increase in electrode-electrolyte interfaces. Although this, the component BCAP010 has a relative capacitance, C_r/C_R, lower than that of BCAP013 because the concentration of impurities per unit area of electrode-electrolyte interface is lower in highest capacitances [7]. These results correspond to those founded by voltamperometry (see fig. 6). The component MC2600 has the highest capacitance, C_r, and the lowest resistances, R_{le}, which signifies this component dissipates an important stored energy compared to that of others. Table 4 illustrates that leakage resistance increases with a decrease of capacitance because membrane surface and quantity of impurities are lower.

Component	BCAP010	BCAP013	BCAP350	MC2600
Capacitance C_R (kF)	2.6	0.45	0.35	2.6
R_r (Ω)	58.1	291	384	45.2
C_r (F)	201	47.4	38.8	367
C_r/C_R %	8	11	11	14
Manufacturer leakage resistance (R_{lem}) (kΩ)	0.50	0.83	2.5	0.54
R_{le} (kΩ)	1.34	4.99	8.0	0.73
R_{le}/R_{lem} %	269	599	321	135
R_{le}/C_R (Ω/F)	0.52	11.1	23.0	0.28

Tab. 4: Self-discharge parameters of studied electrochemical capacitors

6. EFFECT OF VOLTAGE AND TEMPERATURE ON SUPERCAPACITOR PARAMETERS

The supercapacitors can operate in a temperature range as wide as -35 °C to 65 °C. In fig. 18, we show the self-discharge rate for a temperature of -25 °C, 0 °C, 25 °C, 45 °C and 65 °C and for an initial voltage of 1 V, 1.5 V, 2 V, and 2.5 V.

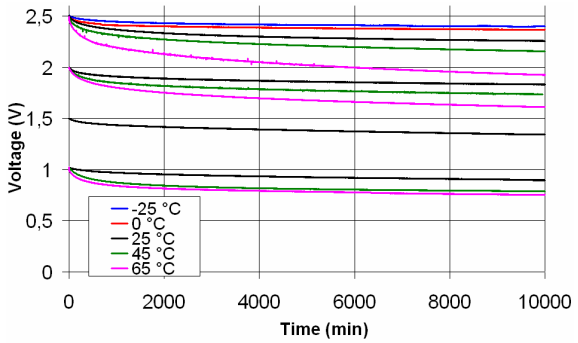

Fig. 18: Self-discharge rate vs. time for different initial voltages and temperature (for component BCAP010)

The dependence of the self-discharge parameters, C_r and R_{le}, on both the temperature and on the initial voltage across the supercapacitor can be shown in fig.19 and 20.

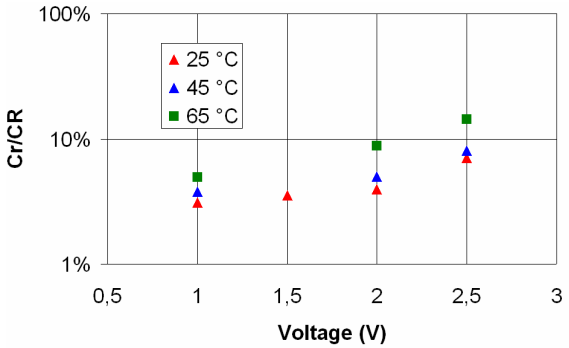

Fig. 19: Variation of C_r v. temperature and initial voltage

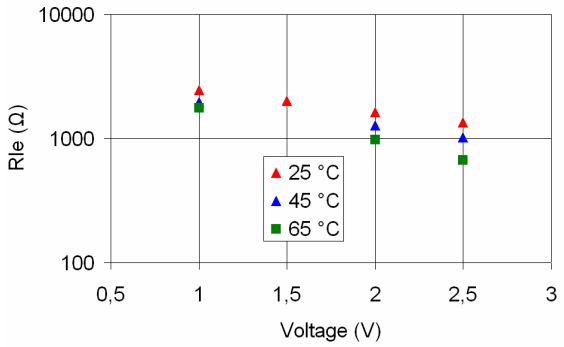

Fig. 20: Variation of R_{le} v. temperature and initial voltage

Consequently, because self-discharge rates are dependent on the rates of ionic transport [16], the self-discharge rates accelerate strongly with an increase in temperature or in initial voltage.

The impedance measurements are performed by EIS at different DC potentials (0 V, 0.5 V, 1V, 1.5 V, 2 V and 2.5 V), and different temperatures (-25 °C, 0 °C, 25 °C, 35 °C, 45 °C, 55 °C and 65 °C). Fig. 21 (a and b) shows the variation of supercapacitor parameters versus the temperature and voltage.

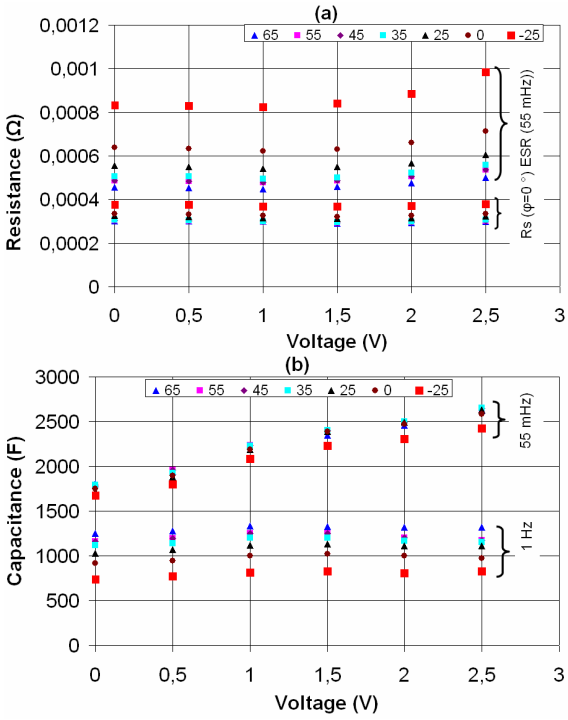

Fig. 21: Supercapacitor parameters vs. temps and voltage

From these results, we can observe: The resistance, R_s, varies lightly with temperature. The resistance, *ESR*, varies as a function of voltage and temperature. The capacitance, C_{dl}, is dependent only on DC voltage and non variation with temperature. By using the transit techniques (charge/discharge, and voltamperometry), we founded a light dependence of capacitance on temperature. The difference between the discharge and charge capacitance (coulumbic efficiency) increases with a temperature decreasing.

In fig. 10 we show the variation of coulumbic efficiency versus temperature for the different current charge/discharge.

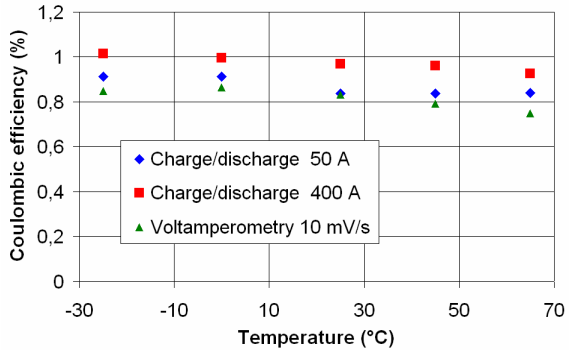

Fig. 22: Coulombic efficiency vs. temperature for different current charge/discharge

This result can be interpreted by impact of temperature on redox. In negative temperatures with fast charge/discharge the redox is deactivated. So, the coulumbic efficiency is almost 100%. In high temperatures with low charge/discharge (as by voltamperometry), it is very low (77%).

7. CONCLUSION

Supercapacitor parameters (R_s, R_{el}, C, coulumbic efficiency, self-discharge) are complex functions of voltage, time, and temperature. We studied the supercapacitor characteristics as a function of current, voltage, frequency and temperature by the help of different characterisations techniques and a comparative study is performed. Self-discharge with diffusion-controlled is modelled in both the time and frequency domain as well as the pseudo-inductance.

The different presented resultants were validated for all the studied supercapacitor.

REFERENCES

[1] P. Kurzweil , B. Frenzel , and R. Gallay, "Capacitance Characterization Methods and Ageing Behaviour of Supercapacitors," *The 15th International Seminar On Double Layer Capacitors*, 2005.

[2] D. IEC, "62391-1, Fixed electric double layer capacitors for use in electronic equipment," *Part I: Generic specification (IEC 40/1378/CD: 2003), June*, 2004.

[3] D. IEC, "62391-2, Fixed electric double layer capacitors for use in electronic equipment," *Part I: Sectional specification: Electric double layer capacitors for power application (IEC 40/1379/CD: 2003), June*, 2004.

[4] L. Zubieta and R. Bonert, "Characterization of double-layer capacitors (dlcs) for power electronics applications," *Industry Applications Conference, IAS Annual Meeting IEEE*, vol. 2, 1998, pp. 1149-1154.

[5] P. Kurzweil, M. Chwistek, and R. Gallay, "Electrochemical and Spectroscopic Studies on Rated Capacitance and Aging Mechanisms of Supercapacitors Based on Acetonitrile," *Proc. 2nd European Symposium on Super Capacitors & Applications*.

[6] W.G. Pell and B.E. Conway, "Analysis of power limitations at porous supercapacitor electrodes under cyclic voltammetry modulation and dc charge," *Journal of Power Sources*, vol. 96, 2001, pp. 57-67.

[7] S.K. Tripathi, A. Kumar, and S.A. Hashmi, "Electrochemical redox supercapacitors using PVdF-HFP based gel electrolytes and polypyrrole as conducting polymer electrode," *Solid State Ionics*, vol. 177, 2006, pp. 2979-2985.

[8] T. Christen and M.W. Carlen, "Theory of Ragone plots," *Journal of Power Sources*, vol. 91, 2000, pp. 210-216.

[9] T. Christen and C. Ohler, "Optimizing energy storage devices using Ragone plots," *Journal of Power Sources*, vol. 110, 2002, pp. 107-116.

[10] S. Buller et al., "Modeling the dynamic behavior of supercapacitors using impedance spectroscopy," *Industry Applications Conference, 2001. Thirty-Sixth IAS Annual Meeting. Conference Record of the 2001 IEEE*, vol. 4.

[11] D. Riu, N. Retiere, and D. Linzen, "Half-order modelling of supercapacitors," *Industry Applications Conference, 2004. 39th IAS Annual Meeting. Conference Record of the 2004 IEEE*, vol. 4, 2004.

[12] E. Karden, S. Buller, and R.W. De Doncker, "A frequency-domain approach to dynamical modeling of electrochemical power sources," *Electrochimica Acta*, vol. 47, 2002, pp. 2347-2356.

[13] J. Bisquert, H. Randriamahazaka, and G. Garcia-Belmonte, "Inductive behaviour by charge-transfer and relaxation in solid-state electrochemistry," *Electrochimica Acta*, vol. 51, 2005, pp. 627-640.

[14] B. Savova-Stoynov and Z.B. Stoynov, "Analysis of the inductance influence on the measured electrochemical impedance," *Journal of Applied Electrochemistry*, vol. 17, 1987, pp. 1150-1158.

[15] E. Harzfeld,, R. Gallay, and M. Hahn, "Capacitance and Series Resistance determination in high power ultracapacitors," ESSCAP, Belfort/France, 2004.

[16] B.W. Ricketts and C. Ton-That, "Self-discharge of carbon-based supercapacitors with organic electrolytes," *Journal of Power Sources*, vol. 89, 2000, pp. 64-69.

[17] B.E. Conway, W.G. Pell, and T.C. Liu, "Diagnostic analyses for mechanisms of self-discharge of electrochemical capacitors and batteries," *Journal of Power Sources*, vol. 65, 1997, pp. 53-59.

[18] B.E. Conway, *Electrochemical Supercapacitors: Scientific Fundamentals and Technological Applications*, Kluwer Academic/Plenum Publishers, 1999.